LRP 439/91 **October 1991**

Plasma Rotation and Radial Electric Field with a Density Ramp in an Ohmically Heated Tokamak

B.P. Duval B. Joye B. Marchal

Submitted for Publication
Nuclear Fusion

Plasma Rotation and Radial Electric Field with a Density Ramp in an Ohmically Heated Tokamak

B.P. Duval B. Joye B. Marchal

Centre de Recherches en Physique des Plasmas
Association Euratom-Confédération Suisse
Ecole Polytechnique Fédérale de Lausanne
Ch-1015 Lausanne, Switzerland

Abstract

Measurements of toroidal and poloidal rotation of the TCA plasma with Alfvén Wave Heating and different levels of gas feed are reported. The temporal evolution of the rotation was inferred from intrinsic spectral lines of CV, CIII and, using injected helium gas, from HeII. The light collection optics and line intensity permitted the evolution of the plasma rotation to be measured with a time resolution of 2ms. The rotation velocities were used to deduce the radial electric field. With Alfvén heating there was no observable change of this electric field that could have been responsible for the density rise which is characteristic of the RF experiments on TCA. The behaviour of the plasma rotation with different plasma density ramp rates was investigated. The toroidal rotation was observed to decrease with increasing plasma density. The poloidal rotation was observed to follow the value of the plasma density. With hard gas puffing, changes in the deduced radial electric field were found to coincide with changes in the peaking of the plasma density profile. Finally, with frozen pellet injection, the expected increase in the radial electric field due to the increased plasma density was not observed, which may explain the poorer confinement of the injected particles. Even in an ohmically heated tokamak, the measurement of the plasma rotation and the radial electric field are shown to be strongly related to the confinement. A thorough statistical analysis of the systematic errors is presented and a new and significant source of uncertainty in the experimental technique is identified.

1. Introduction

The original stimulus for measuring the radial electric field on TCA was the large density rise observed with high power Alfvén Wave Heating (AWH) [1]. TCA is a medium sized Tokamak (R=0.61m a=0.18m, Ip=130kA) [2] and the density rise has previously been found to be proportional to the RF power [1]. Various possible explanations for this density rise have been proposed and subsequently rejected. Successive reductions in the impurity levels in the plasma bulk have proven that the particle influx is not due to impurities but rather to the working gas [1]. Conditioning of the machine walls resulted in a considerable increase of the edge recycling, but this did not change the

density rise with RF heating. Since the density rise does not appear to depend on the machine wall, a change in one or more of the parameters which determine the plasma confinement is indicated.

Recently, there has been considerable interest in the behaviour of the radial electric field in the edge of a Tokamak plasma during the transition to H mode [4, 5]. The large edge gradient of the radial electric field in the H-mode is thought to be responsible for the improved particle confinement. Conversely, the reduction of the radial electric field observed in the L-mode [4], could explain the degradation of the confinement. By driving a radial current across the outer magnetic surfaces using polarised edge probes, a transport barrier with similarities to other H-mode observations has also been achieved [6]. Since Stringer [7] showed that poloidal rotation in a toroidal plasma resulted in an increased radial diffusion, there have been several, and sometimes contradictory, models of the effect of a radial electric field on the plasma confinement. These models, and the growing number of experimental observations, imply that a change in the radial electric field could lead to changes in the radial diffusion or particle confinement. Impurity ablation experiments on TCA [8] indicate that there is a change in the particle confinement time during the RF induced density rise. The initial goal of the rotation experiments on TCA was thus to determine whether there is a change in the radial electric field which accompanies the RF induced density rise.

During the operational period of this diagnostic, there was an extensive experimental campaign to study high density discharges achieved by very strong gas puffing [9]. In these discharges, high densities were achieved by a fast density ramp rate. A major plasma disruption was often observed if the density ramp rate was too low which seems to be suppressed by forced gas puffing. Although the initial interest in the discharges was to examine the effect of a strong density rise on the plasma ion velocity, as accompanies AWH, some additional data were observed that merit being presented in their own right. To complete the study of different rates of density rise, measurements of the plasma rotation during frozen pellet injection are described. The density rise resulting from pellet injection is extremely abrupt, and the behaviour of the toroidal rotation, and thus the deduced radial electric field, was quite different from during the other observations.

The measurement of the toroidal plasma rotation is also of interest since it is required to infer the radial electric field. It is also currently employed in the measurement of the plasma viscosity via a measurement of the rate of change of the toroidal velocity induced by momentum injected from tangential high power neutral ion beams. Although such beams were not available on TCA, the behaviour of the toroidal rotation in an ohmically heated plasma under the above conditions is reported and contrasted to the poloidal velocity.

In the first part of this paper the experimental set up is described together with some preliminary results and a detailed analysis of the experimental accuracy. In the second part of this paper the toroidal and poloidal rotation results are presented for RF heating, forced gas puffing and pellet injection, and some conclusions are presented in the final section.

2. Apparatus and Methodology

A 1m Czerny-Turner spectrometer equipped with a 2400line/mm grating was used for all the experimental observations. A PARC 1024 channel blue enhanced multichannel diode array detector was mounted in the spectrometer's image plane [10]. The acquisition electronics allowed a complete spectral profile of the desired atomic transition to be acquired every 2ms and a complete scan of the full 1024 diodes in the OMA every 16.6ms. It was this limitation in the read out electronics, rather than the intensity of the observed spectral features, which limited the obtainable temporal resolution.

The light collection optics and the lines of sight used are shown schematically in Figure 1. Light is collected through an f1 telescope with a 25mm beam diameter from the TCA plasma. The telescope is connected via a 1.25 mm diameter fibre-optic light guide to a multi-fibre carousel on the entrance slit of the spectrometer. This system permits one of 6 fibres to be kinematically selected on a shot to shot basis. The whole optical path was equipped with quartz elements and the optical paths minimised to maintain over 50% transmission from the telescope to the spectrometer down to the

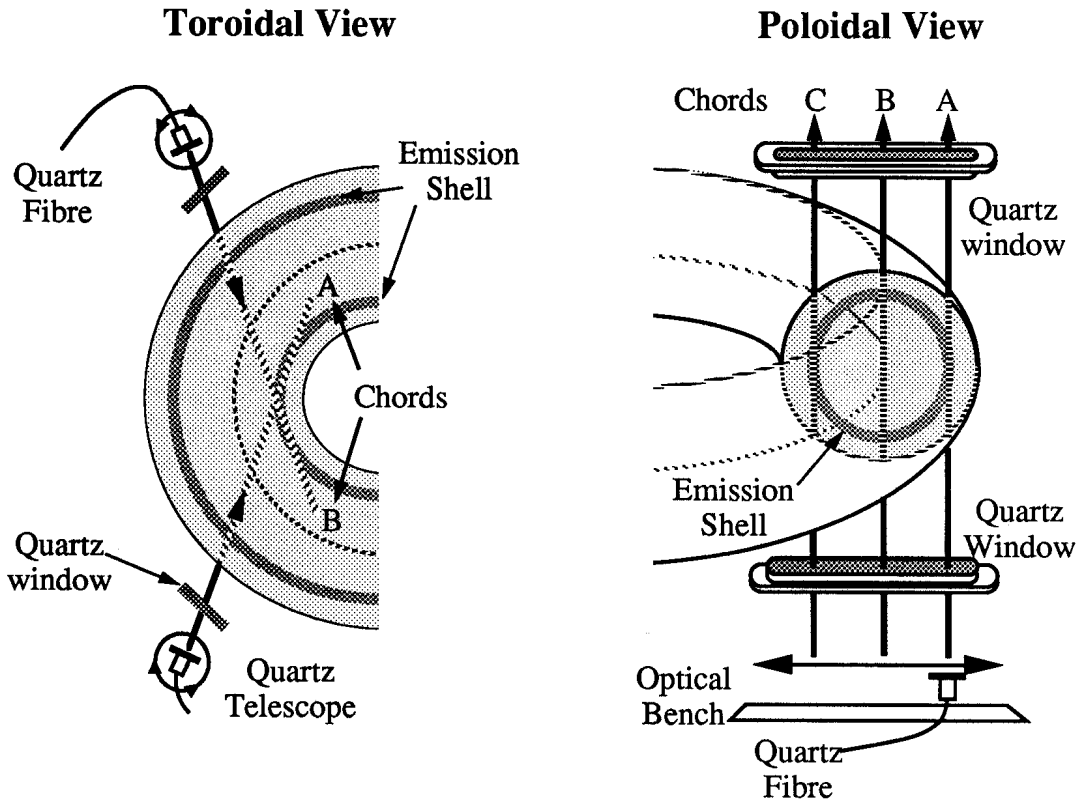

Figure 1: Schematic of the position of the telescopes used for the rotation measurements. a) For the toroidal view, the inner minor radius was observed in and against the plasma current direction. b) For the poloidal view, optimal vertical chords through two slot ports were used, which reduced the effect of reflections, and permitted a scan of the poloidal velocity across the minor radius. In both figures, the emission zone of a typical spectral line is shown together with the telescope line of sights. Chord A was used for the measurement and chords B and C for the calibration.

shortest observed wavelength of 227nm.

TCA is equipped with graphite limiters and carbon is thus an intrinsic impurity. The spectral purity and the intensity of CV at 227.0nm and CIII at 229.5nm made them natural choices for the rotation experiments. Figure 2 shows the measured TCA plasma light emission around these lines which are seen to be unpolluted by nearby spectral features and quite intense. The emission of these spectral lines in TCA takes the form of a shell which peaks at minor radii of r/a ~11/18 and r/a ~16/18 respectively. The rotation can thus be investigated as a function of minor radius from these two measurements, although not with the same spatial resolution as would be obtained by a crossed beam technique e.g. the spectral emission from charge exchange recombination using an injected neutral beam [11]. These spectral lines were observed in second order, which, with the ~37μm effective width of the OMA diodes, limited the spectral resolution to ~0.006nm. Since these spectral lines exhibit considerable Doppler broadening, an entrance slit of 50μm was commonly used to improve the light throughput, without introducing any significant instrument broadening. During the experimental period, the machine vessel was regularly conditioned by boronisation which significantly reduces the Carbon impurity content [12]. During these periods, auxiliary observations were performed using a HeII spectral feature (468.5nm) viewed in first order by injecting Helium gas into the plasma discharge. For this measurement, the spectral resolution was ~0.01nm. This spectral feature is emitted from near the same minor radius as CIII which permitted an investigation of any element specific behaviour and a comparison with other experiments which often use this spectral feature [13] [14] [15]. The spectral emission from TCA around this line is also shown in Figure 2.

It is important to note the main feature of the experimental set up. For the poloidal measurements which, as will be shown below, dominate the measurement of the radial electric field, the plasma was viewed through opposing slot windows above and below the plasma vessel. By choosing an appropriate vertical chord for each spectral feature observed, the poloidal rotation was

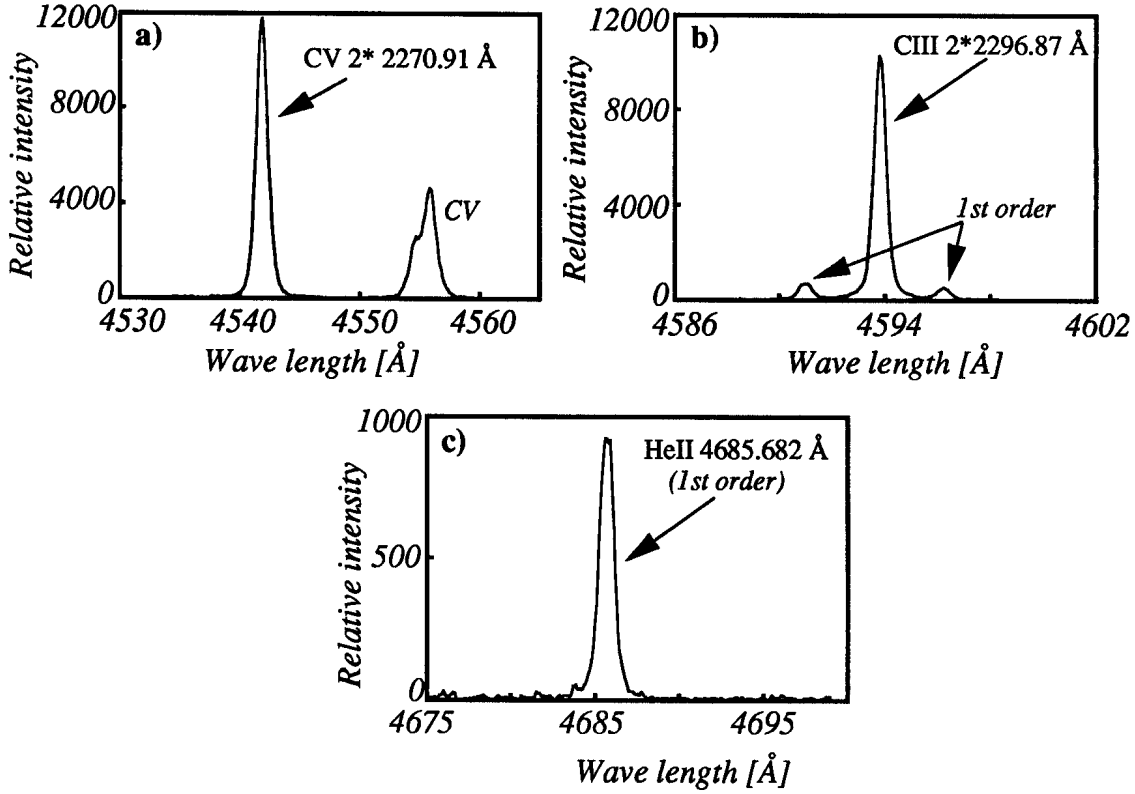

Figure 2: *a) The spectral emission from TCA around the CV line in second order (227.1nm). b) The spectral emission around the CIII line in second order (229.7nm) where some first order features are also seen, but do not interfere. c) The spectral emission around the HeII line in first order (468.6nm). All three spectral features are intense and unpolluted by other spectral features.*

always observed tangentially and with very little pollution from reflected light. This translates into an extreme purity of the observed spectral profiles which improves the experimental accuracy. By scanning this vertical axis across the minor axis, the poloidal rotation is measured as a function of minor radius.

The radial electric field is deduced from the first order force balance equation for the ions:

$$E_r = \frac{1}{n_i Z_i e}\frac{\partial p_i}{\partial r} - v_\theta B_\phi + v_\phi B_\theta \qquad (1)$$

where (r,θ,ϕ) are the usual toroidal co-ordinates, and the subscript refers to an ion i of charge Zi, density ni and a pressure profile pi. The importance of the ion pressure gradient term is described later. The importance of the remaining terms depends on the measured velocities and the ratio of toroidal to poloidal magnetic field. The q profile has been measured in TCA for a range of plasma currents using driven Resonant Alfvén waves [16]. From the measured current profile at Ip=130kA, the ratio between $B\theta/B\phi$ is ~10 for all the observed spectral features. Thus, in situations where the pressure gradient term is not significant and the poloidal and toroidal velocities have the same magnitude, the measurement of a change in radial electric field reduces to a satisfactory measurement of the poloidal rotation.

This determination of the absolute velocity depends on a very accurate measurement of the observed line profile, and special care is required to maintain an acceptable calibration. Two calibration techniques were used to determine the absolute rotation velocity for the toroidal and the poloidal measurements. In the toroidal direction, the plasma was viewed parallel and anti-parallel to the plasma current from shot to shot. A measurement of the line position relative to a spectral reference lamp feature was also performed. In the poloidal direction, the velocity was measured along a vertical chord tangential and orthogonal to a poloidal rotation from shot to shot (Figure 1)

and again a comparison was made relative to a spectral lamp.

In preliminary observations using this spectral lamp, the central position of the diffracted image on the OMA was found to vary considerably over a period of hours. Since the form of this drift was repeated on a daily basis, thermal expansion of the spectrometer was suspected to be responsible. The drift was considerably reduced by thermally insulating the spectrometer using an isothermic blanket but not sufficiently for this effect to be neglected. The residual temperature changes were monitored with an array of thermistors distributed around the spectrometer and glued directly onto the spectrometer chassis. These temperatures and the centroid position of the reference line from the spectral lamp were monitored regularly as a function of time. By applying the calibrated correction deduced from these measurements, the effect of thermal drift on the accuracy of the rotation measurement was reduced to less than 25% of the uncertainty measured during these experiments. In a similar effort to reduce systematic sources of error, the entire spectrometer was mechanically decoupled from its mount using metallic springs. This considerably reduced mechanical vibration transmitted through the ground to which the spectrometer's grating mount was known to be sensitive.

3. Preliminary Results and Error Analysis

The measurements reported here require an extremely precise determination of the spectral profile, since changes in the deduced electric field depend on small changes in this profile. Therefore, it is pertinent to analyse the experimental accuracy of the measurements. Typically, a spectral profile is integrated on the OMA for 2ms and then acquired. Figure 3a shows such an acquired line profile for CV viewed in the toroidal direction together with a gaussian least-squares fit. The spectrometer's instrument function was measured and can also be deconvolved by the fitting routine. In Figure 3b, the time evolution (i.e. the fit parameters every 2ms) of the spectral width and position of the CV line are shown in OMA pixels for the 120 profiles taken during the plasma discharge. Figure 3b also shows the inferred toroidal rotation velocity and the ion temperature corrected for the spectrometer's instrument function.

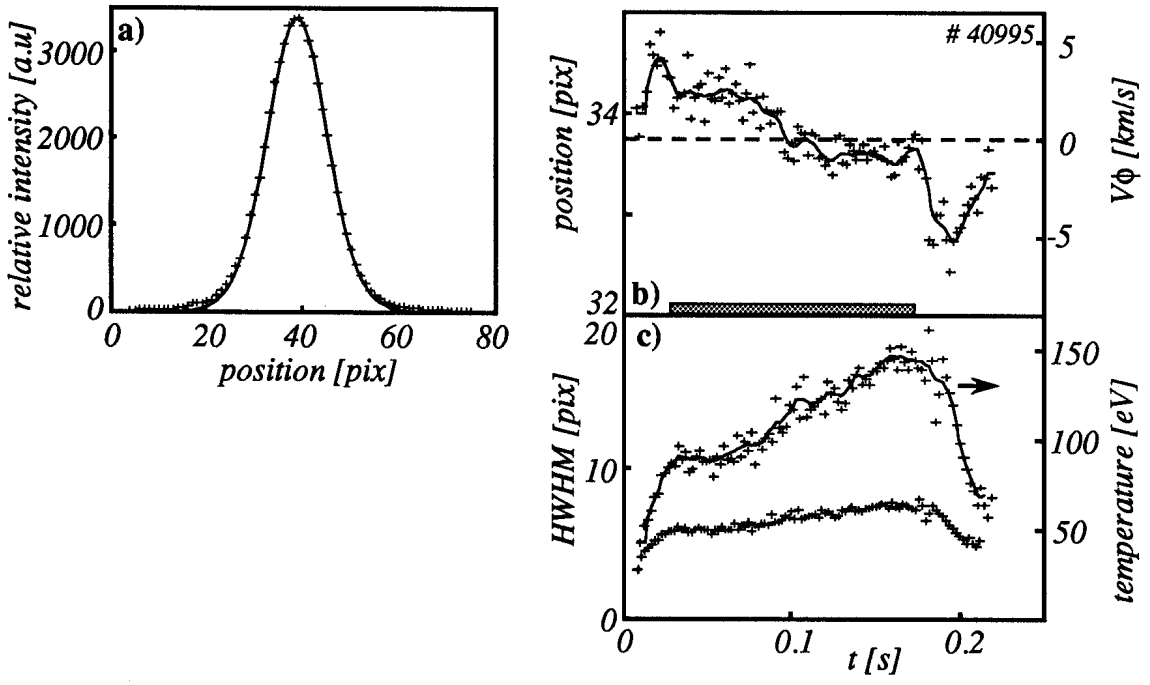

Figure 3: a) The spectral profile of the CV line integrated for 2ms on the OMA detector, together with a least squares fitted gaussian profile. b) The temporal evolution of the fitted gaussian centroids through a plasma discharge in pixels and shown as a toroidal rotation velocity. The solid line was obtained by passing the experimental points through a low pass filter and the solid rectangle represents the region of plasma current flat top. c) The evolution of the fitted gaussian HWHM, for the same discharge, which is also expressed as an ion temperature.

The spectral line profile is very pure and the count rate sufficient for shot noise to be negligible. The scatter in this data was significantly higher than expected from the calibration data. It is important to recall that an accuracy of 0.5km/s in the measured velocity for CV corresponds to a measurement of the line centre to better than 1% of its FWHM. To achieve this precision, it is necessary to examine the mechanisms that could systematically affect the spectral line profile. The central line position was determined using two techniques. In the first technique, as mentioned above, a gaussian profile was fitted in a least squares sense to the data and the central position estimated. This method requires that the line profile be gaussian, and any deviations from this profile can affect the result. In a simpler analysis, if the line profile maintains the same degree of symmetry around the line centre, the central position can be extracted from the curve centroid i.e. the position at which the integrals of the profile on both sides are equal. This has the advantage of being able to treat all profiles, including, of course, a gaussian profile. In all the TCA experiments, the two methods yielded values well within the error margin, which is a direct result of the quality of the line of sight that was used. In the remainder of this paper, only the results of the least squares fit will be presented, although the deduced rotation was routinely compared with that obtained using the centroid method.

The statistical uncertainty of the velocity measurement was investigated by analysing the toroidal rotation measured during the plasma current flat top for a sequence of similar discharges where the toroidal velocity was observed to evolve slowly in time. This analysis was performed in two steps. Firstly, the locus of the deduced centroid position during the discharge was heavily smoothed. Then the deviation probability of the fitted centroids from this smoothed curve was calculated. This method of extracting the experimental uncertainty relies on the fluctuations of the measured velocity being in a different frequency range from that of changes in the real rotation velocity. The fast component of the velocity is removed by the smoothing (i.e. a low pass filter) and the probability curve, Figure 4a, shows the deviation from the smoothed curve, which is assumed to be close to the actual value of the toroidal rotation. To determine any dependence on the line intensity, the data is replotted in figures 4b and 4c according to the plasma density which is approximately proportional to the line intensity. The uncertainty is seen to depend on the emission intensity falling from s~680m/s to s~420m/s for the higher line intensities.

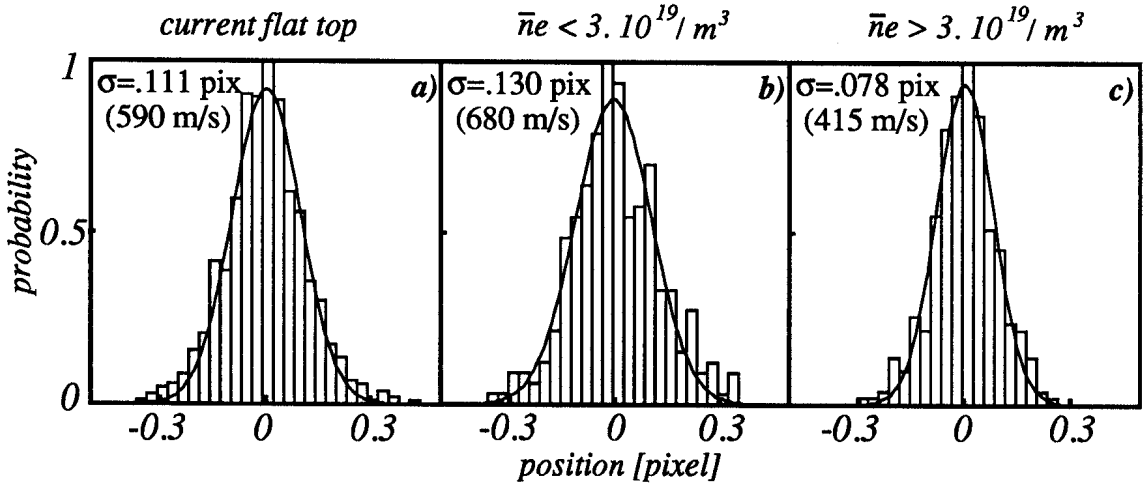

Figure 4: For a sequence of similar shots, and during the plasma current flat top, the spread of the fitted centroid residuals is shown in histogram form for a) All plasma densities, b) at low plasma density $n_e < 3 \times 10^{19}/m^3$, c) at high plasma density $n_e > 3 \times 10^{19}/m^3$. The HWHM of these distributions is also shown in pixels and expressed as a statistical error in the fitted centroid position. See text.

This uncertainty is far larger than the value of s~120m/s obtained by measuring the centroid of an emission line from the spectral lamp in the same conditions i.e.through a TCA discharge. This eliminates the possibility that the larger uncertainty obtained when observing light from the plasma is due to an effect of the discharge on the instrumentation. The extreme sensitivity to the spectral line shape can make any possible line profile change due to the emission processes from a tokamak important. Many possible mechanisms have been suggested in other measurements of the line position, (see [15] for a good selection), which mostly depend on the ion excitation mechanism,

observation angles and electromagnetic fields in the observation region.

During the analysis of these experiments, a new, and distinctive, mechanism was identified which is a result of using an OMA detector and should thus be present in many other measurements which also use an OMA style detector. To understand this mechanism, it is necessary to examine in detail the operation of an OMA detector. The OMA consists of a linear array of diodes which are sequentially read out with 2ms between successive reads. In fact the integral of the light which has fallen on the diode since the last time it was read out is measured. Since all the diodes in a given spectral profile are not read out and acquired simultaneously, a spectral profile is made up of pixels which are staggered in time to each other. This does not lead to a distortion of the measured profile if the incident light intensity is constant. If, however, while the OMA is being read out there is a variation in the incident line intensity, the integral of this variation will be registered in all the subsequently read out pixels. Some of these pixels will be associated with the next spectral profile acquired e.g. if when the intensity fluctuation starts pixel 50 of a 100 pixel profile is being acquired, the effect on pixels 1-49 will only be observed during the next acquired profile.

To clarify the effect of this process on an acquired line profile, the results of a simulation code are shown in Figure 5. This simulation assumes an incident spectral line intensity with a purely

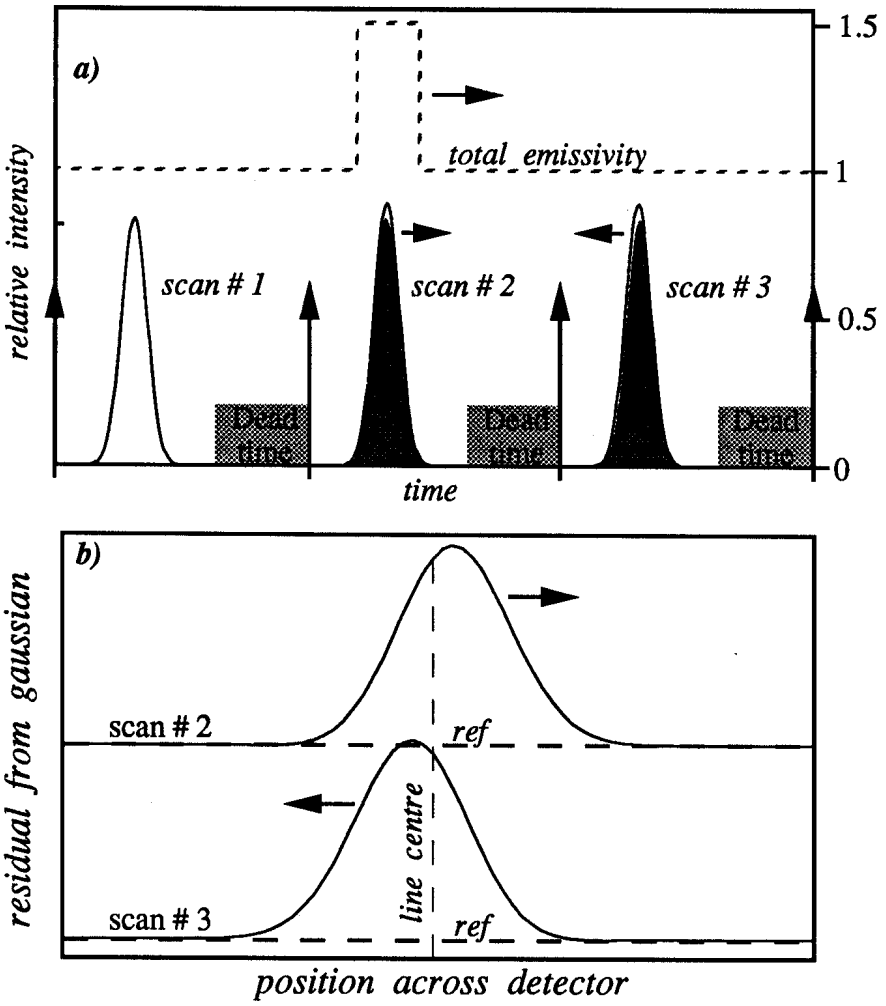

Figure 5: Results of a simulation code to show the effect of an intensity fluctuation on the fitted centroids. a) The total line intensity of a spectral feature with a pure gaussian line profile is shown. Together is shown the simulated spectra, on the same time scale, where dead time between scans is indicated. Scan #1 has a purely gaussian profile. Scan #2 is more intense, with a centroid displaced towards the end of the OMA indicated by an arrow. Scan #3 is also more intense than Scan #1, with a corresponding shift towards the start of the OMA. Scan #1 is used as a reference and is shown in grey underneath Scans #2 and #3 to highlight the effect. b) Using Scan #1 as the reference, the profiles of Scan #2 - Scan #1 and Scan #3 - Scan #1 are shown across the detector with a vertical line at the position of the reference's centroid. Arrows indicate the direction in which the fitted centroid will be displaced for these profiles.

gaussian line profile, constant line width and a constant centroid position i.e. no rotation velocity. In Figure 5a, a plot of the total spectral line intensity is shown together with the intensity of the acquired pixels on the same time scale. Between the last pixel of an acquired profile and the start of a new profile, there is a dead period where the acquisition performs some housekeeping tasks, which is also shown.

During the first simulated profile, the incident intensity was constant, and the simulated profile is gaussian. This profile is used as a reference for the remainder of this discussion. During the read out of the second profile, the incident line intensity has a short period of increased intensity, the effect of which is seen on the next two simulated profiles. Although the integrated intensity during the whole simulation has a gaussian profile, the intensity from the transient is not distributed symmetrically about the true profile centroid. The profile being read out during the jump will thus appear to have its centroid shifted towards the end of the OMA array, whereas the subsequently read profile will have a corresponding shift towards the start of the OMA array. The effect on the centroid position of such a jump is greatest when it occurs as the central pixel of a profile is being acquired, and least important when a pixel in the profile wings is being read out. To highlight this effect, the reference profile is redrawn for the second two scans in Figure 5a). In Figure 5b) the difference between the second two scans and the reference profile is plotted together with the position of the true centroid. By analogy, a reduction of the total light intensity would cause the effect to be reversed. Thus, in the observation of a Tokamak plasma where there may be a fluctuating total line intensity, this process will be seen as an additional source of line centroid uncertainty.

It now remains to be shown that this mechanism is indeed important in the experiments on TCA. The effect of this mechanism is to spread a change in line intensity between adjacently acquired profiles. One of these will show a centroid shifted towards the start of the OMA and the other towards the end of the OMA. The existence of this effect is demonstrated in Figure 6 which shows the evolution of the fitted centroids for CV toroidal observation using three algorithms. Each fitted sequence is shown together with the auto-correlation of the residuals i.e. the auto-correlation of the

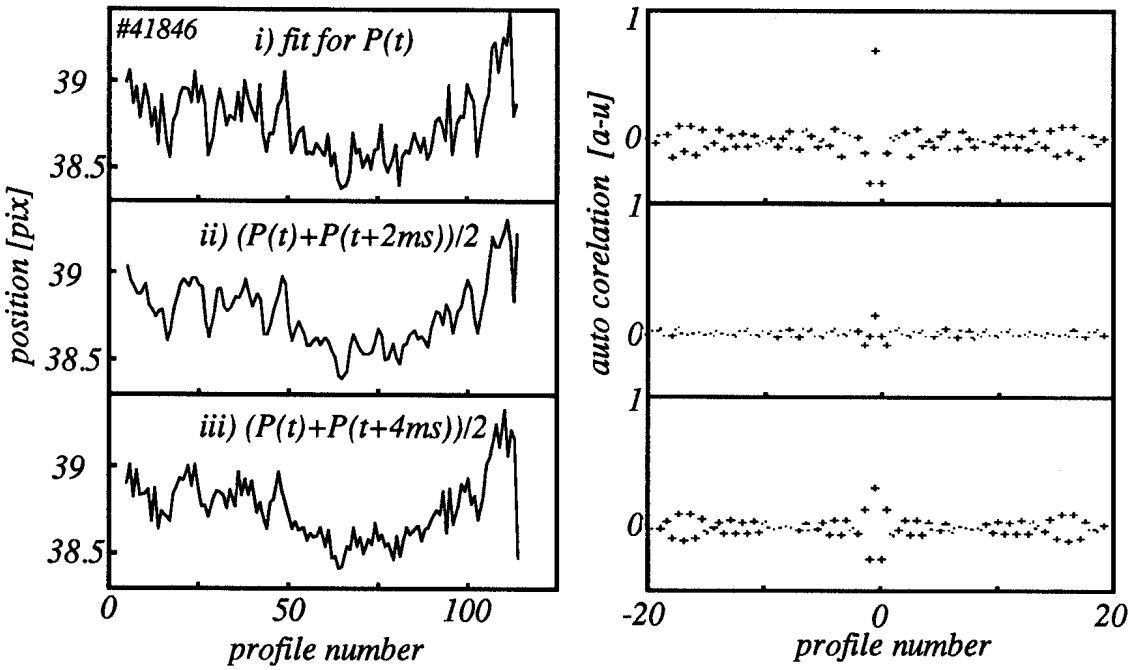

Figure 6: *a) Three algorithms were used to fit the 120 measured profiles from CV during TCA discharge #41846. i) Each profile is fitted separately. ii) Adjacent profiles are added before fitting. iii) Each profile is averaged with the one after next before fitting. The curve with the adjacent averaging is clearly the most smooth. b) The cross correlation functions for the three curves in a) are also shown. i) There is a significant negative correlation between adjacent pairs i.e. +/- 1 profile. ii) The cross correlation is significantly reduced. iii) Again strong cross correlation is visible together with the effect of the averaging algorithm. See text.*

residuals as calculated for Figure 4. These cross correlation functions shown are for the fast fluctuations of the velocity around a smoothly evolving rotation velocity, which was extracted as for Figure 4.

In Figure 6a, the fit is performed on the raw data. The auto-correlation, apart from the normal peak at t=0, has a large and negative value at t=+/-1 profile. This suggests that the residuals are correlated in anti-phase between adjacent pairs of profiles which is predicted for the mechanism described above. For the centroid evolution in Figure 6b, adjacent profiles were averaged before the fit was performed. The evolution of the fitted centroid is much smoother and the autocorrelation of the residuals greatly diminished. To show that this is not simply the statistical improvement due to averaging two noisy spectra, Figure 6c shows the fitted centroids after averaging a profile with one after next. The fitted position is not smoother than in Figure 6a and the auto-correlation function again shows evidence of an adjacent correlation together with the effect of the averaging function itself, as predicted by the model.

By taking the mean of adjacent profiles, the effect of an intensity fluctuation common to the two profiles will cancel, which results in a reduction in the observed uncertainty. Although this does not actually deconvolve the effect of an intensity fluctuation, the resulting smoothness of the fitted

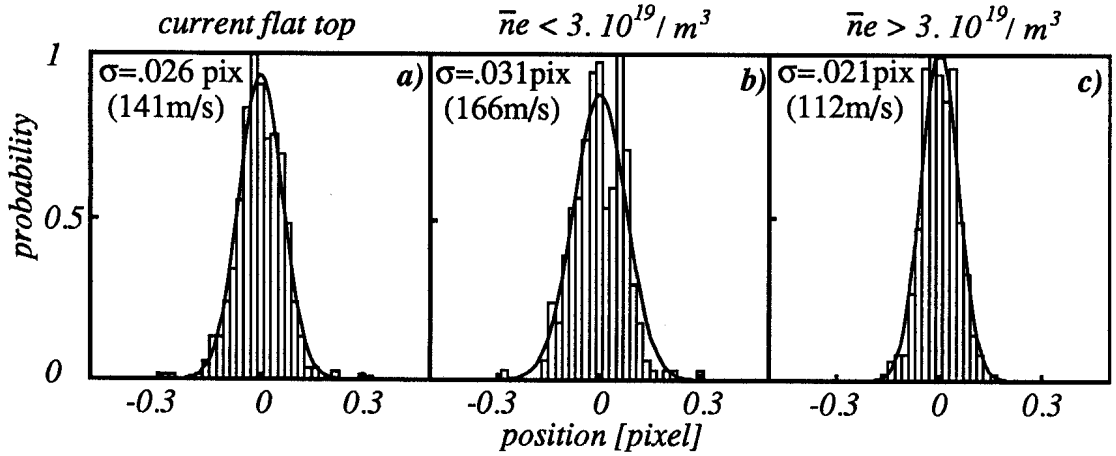

Figure 7: For the same data used in Figure 4, the spread of the fitted centroid residuals are again shown, but after using the adjacent averaging algorithm. The HWHM of the distributions is again shown in pixels as a statistical uncertainty of the measured velocity. The residual uncertainty was reduced to the value obtained from an observation of the reference spectral lamp through a TCA discharge.

position and reduction of the adjacent auto-correlation is clear evidence that this mechanism is important. To deconvolve intensity fluctuations correctly, the incident line intensity would have to be monitored with the same temporal resolution as the OMA pixel acquisition, say with a photomultiplier equipped with an interference filter. The pixels of each profile would then be normalised before the fitting procedure is used to extract the line centroids. It is interesting to note that in an OMA detector, if there is only one spectral feature on the whole detector, this could also be achieved by monitoring the current through the microchannel amplifier plate. Unfortunately, this was not realised before the TCA rotation experiments were completed and could not be performed. During an observation where the line intensity may vary several times during a scan of the OMA, the deviation of the spectral profile from a purely gaussian shape will not be clear, and will more probably be interpreted as a change in the centroid position.

The effect of the adjacent averaging was to reduce the measured uncertainty by up to 70%. This is demonstrated in Figure 7 where the distribution of the residuals is shown for the same discharge as Figure 4, but after averaging. At higher plasma densities, the uncertainty was found to be s~110m/s which compared well with that obtained from the spectral lamp. A modified simulation, used for Figure 5, was found to predict an improvement in the same range. The remaining uncertainty should be considered as the intrinsic error in the apparatus used and is due to spectrometer vibration, read-

out noise and the inadequacy of the correction procedure applied to account for intensity fluctuations etc. The adjacent averaging procedure should not simply be regarded as a statistical smoothing algorithm. The effect it compensates for is intrinsic to the OMA read out system.

4. Toroidal Rotation Results

Light from the inner minor cross section was used for the toroidal velocity measurements (Figure 1). This means that the emission distribution of a spectral line, which is normally peaked at a particular minor radius, is intercepted twice by the line of sight on the outer minor radius as well as on the inner minor radius. If the plasma rotates toroidally with a given angular velocity, the spectral profile observed will thus be a function of the rotation velocity. By comparing the intensity contribution from the inner minor radius to that from the outer minor radius, this effect was calculated to introduce an error of less than 5% in the measured toroidal velocity.

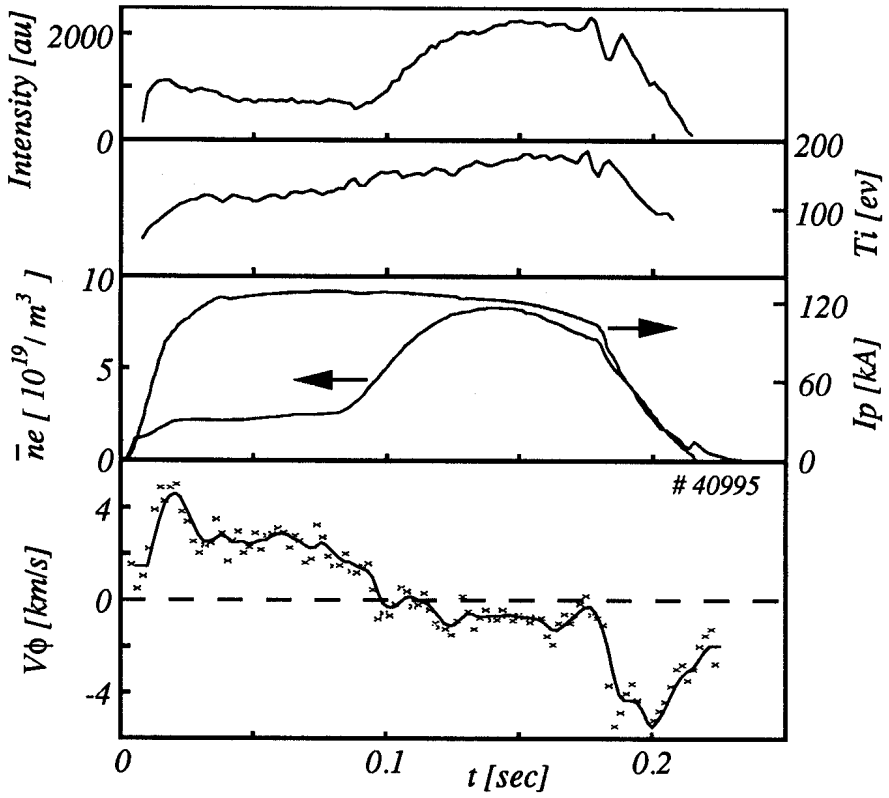

Figure 8: The toroidal rotation velocity measured from CV though a plasma discharge with a density ramp. A positive velocity corresponds to the direction of the plasma current. The plasma current and density are also shown. The rotation velocity decreases with increasing plasma density. During the plasma current ramp down, there is a sharp toroidal acceleration in the opposite direction.

An example of the temporal evolution of the toroidal rotation from CV is shown in Figure 8 through a discharge together with the evolution of the plasma current and line averaged plasma density. This discharge is in fact the same as in Figure 3, but fitted after using the adjacent averaging algorithm. The toroidal velocity is defined as positive in the plasma current direction. After an initial increase during the plasma current build up, it decreases with increasing plasma density. During the plasma current ramp down at the end of the discharge, it speeds up in the other direction until the plasma density has fallen to a low value at which time the plasma ceases to rotate toroidally. Figure 8 also shows the evolution of the fitted ion temperature and line intensity which is approximately proportional to the plasma density. This behaviour was also seen in the plasma edge with CIII and HeII Figure 9a. Here the evolution of the plasma density is also shown and the period of the current flat top indicated. The only significant difference is that the edge toroidal velocity measured from CIII and HeII was observed to change more quickly and before that of CV indicating that the

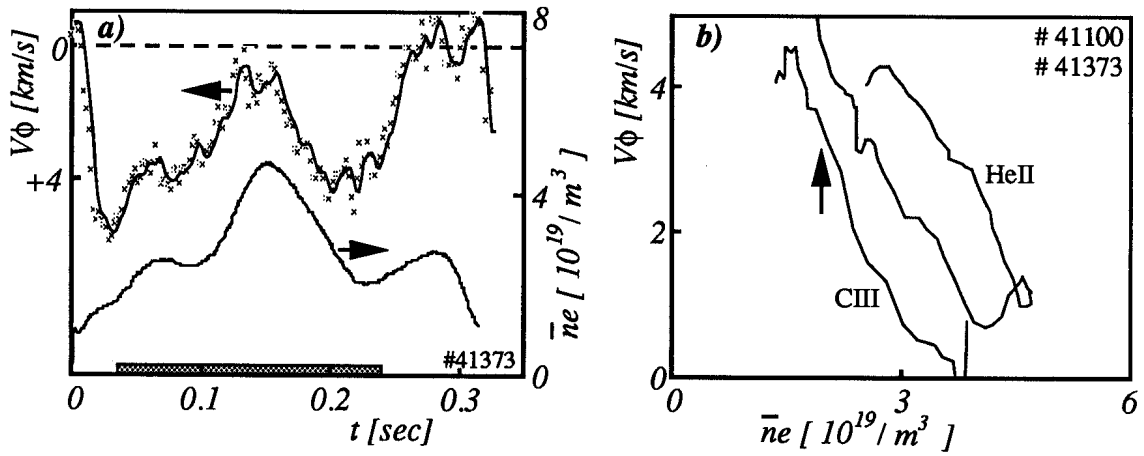

Figure 9: *a) The toroidal rotation measured with HeII is shown for a discharge with a density ramp and fall, where the region of plasma current flat top is indicated by a grey rectangle. During the current ramp down the edge toroidal velocity changes sign. b) Locus of the toroidal rotation in a) as a function of the mean plasma density. The slope during the density ramp and density fall is similar although the locus does not exactly retrace itself. The measured evolution from CIII with AWH is also shown, with the start of RF heating indicated by a vertical arrow. There is no distinctive change observed with AWH.*

acceleration force diffuses in from the plasma edge. This was not the case during the current ramp down where the HeII velocity was less affected than CV indicating that here, the accelerating force was more central.

In Figure 9b, the locus of the velocity is shown against the line averaged plasma density in the current flat top region for HeII and CIII. For the normal gas puff, the velocity measured from He II decreases nearly linearly with plasma density and then recovers as the plasma density falls. The locus as the density falls has the same slope as during the density ramp, but with an offset which shows that the value of the rotation velocity also depends on some other parameter. The toroidal velocity measured from CIII in Figure 9b was measured in a discharge with AWH where the density ramp was caused by the RF power. As the plasma density rises with RF power, the velocity decreases with a slope indistinguishable from that due to the gas puff. In general, the toroidal rotation results did not distinguish between AWH and a normal gas puff. Although the absolute position of the density dependence traced in Figure 9b varies between and even during discharges, the slope was very similar for all the measurements of the edge plasma rotation. This data also shows that there is little dependence of the toroidal rotation on the charge of the observed ion.

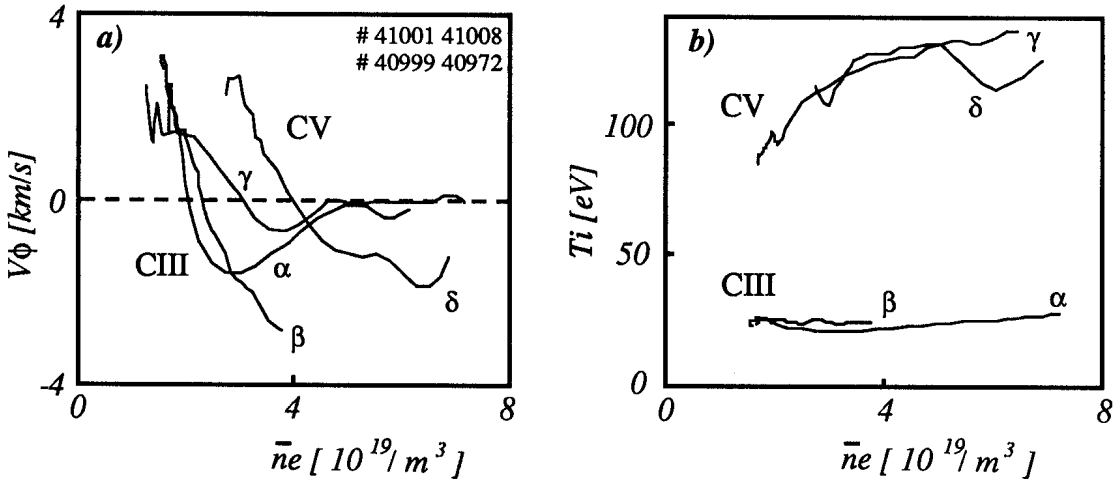

Figure 10: *Summary of the behaviour of the toroidal rotation with different levels of gas puffing. a) the locus of the toroidal rotation evolution against mean plasma density for CIII and CV with normal gas puffing β) and δ) and for hard gas puffing α) and γ) respectively. With normal gas puffing, the velocity changes sign smoothly. With hard gas puffing, the rate of change of the toroidal velocity is higher, but then undergoes a transition which returns the velocity close to zero. b) The ion temperatures for the four discharges in a) as a function of the mean plasma density*

Since the toroidal velocity results are less pertinent to the discussion of a radial electric field, the effect of different strengths of gas feed on the toroidal velocity are summarised in Figure 10 where the measured toroidal velocity is shown for two strengths of gas puffing for both CV and for CIII. The first observation is that the initial trajectory of the velocity evolution changes with harder gas puffing. The velocity falls more quickly than with normal gas puffing and crosses zero. Then, as the density increases further, the rate of change of toroidal velocity with density reverses and the velocity returns to near zero. As with normal gas puffing, these effects are slower and smaller for the more central CV line. Figure 10 also shows the corresponding ion temperatures which appear to simply increase with plasma density as has previously been observed [17]. In conclusion, if the plasma density rises slowly, the toroidal velocity falls and changes sign. If, however, the density rise is faster, the toroidal velocity changes direction more quickly but then stalls.

These results were verified by observing the toroidal plasma rotation in the opposite direction to the plasma current (Figure 1), which confirmed the value of the absolute toroidal velocity. The effect of forced gas puffing is treated in greater detail with the presentation of the poloidal rotation data below.

5. Poloidal Rotation Results

The essence of the evolution of the poloidal rotation velocity with AWH is shown in Figure 11a. A positive poloidal rotation is defined to be in the electron diamagnetic direction. The scales are chosen to underline the main observation that the poloidal rotation velocity follows the plasma density. No discernible difference was observed with AWH compared with a normal gas puff, as was the case for the toroidal rotation results. The same data is shown in Figure 11b where the locus of the

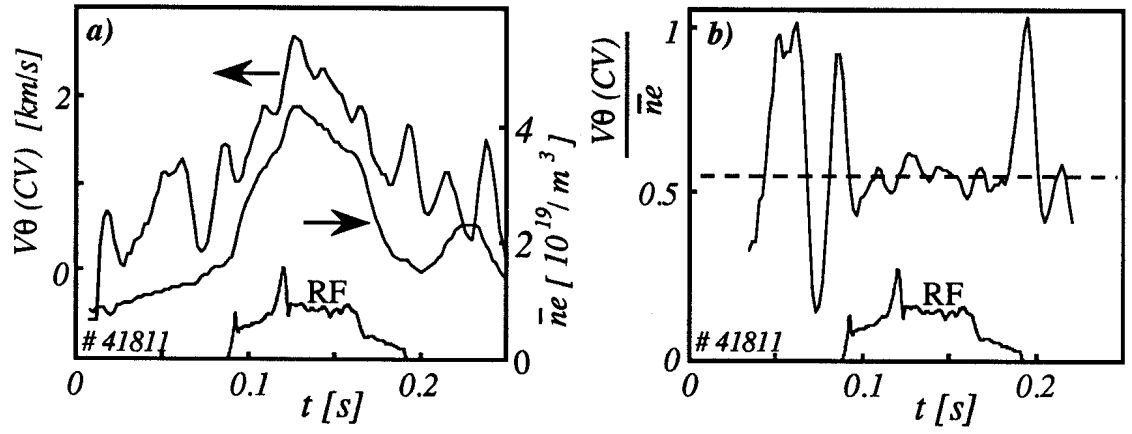

Figure 11: a) The evolution of the poloidal rotation measured from CV with AWH. A positive rotation is defined in the electron diamagnetic drift direction. The axes have been chosen to highlight the observation that the poloidal velocity follows the plasma density. The relative rf power is also indicated b) For the same discharge, the poloidal rotation is shown normalised to the mean plasma density. No change in this normalised rotation velocity is observed with the start of AWH.

poloidal rotation normalised to the plasma density is plotted. The variations in this ratio at the start and end of the discharge occur during the plasma density ramp up and current ramp down respectively. With the onset of AWH there is no jump in the normalised poloidal velocity. Since the absolute value of the toroidal rotation is observed to decrease with increasing plasma density, (1) indicates that the radial electric field is dominated by the increasing poloidal rotation. There is thus no jump in the radial electric field which occurs co-incidentally with AWH.

The estimated radial electric field during a density ramp is shown in Figure 12 together with the poloidal rotation. The shaded region on this graph is an estimation of the uncertainty due to the

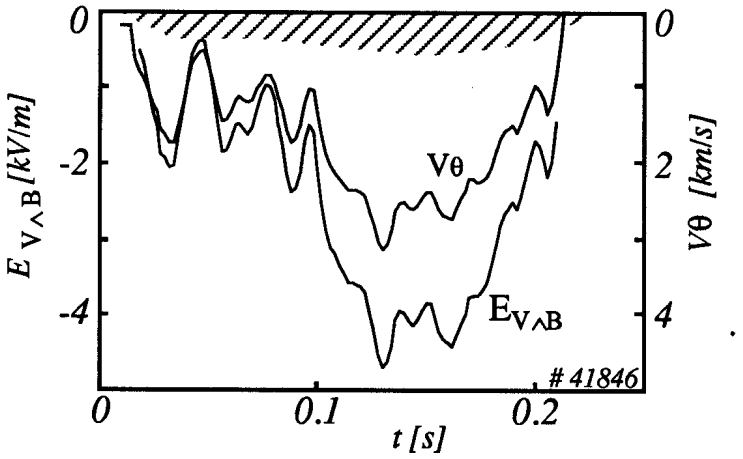

Figure 12: The poloidal rotation is shown for a discharge with a density ramp together with the deduced radial electric field. The curve is corrected for the small effect of the toroidal velocity, and the maximum estimated uncertainty in the absolute electric field due to ion pressure gradient term in Eqn 1 is shown by the shaded region.

ion pressure gradient term for CV (1), where the ion temperature is assumed to be constant and the pressure only depends on the ion density. The same effect was observed for CIII and HeII, although, as for the toroidal rotation, the edge poloidal rotation is greater and changes faster than that measured from the more central CV radiation. Figure 13 summarises these observations together with some data obtained during hard gas puffing. The toroidal velocity is shown for CV (Figure 13a) and for HeII (Figure 13b) together with the measured ion temperatures (Figure 13c) as a function of the line averaged plasma density. The shaded regions in figures 13a and 13b indicate the range of values

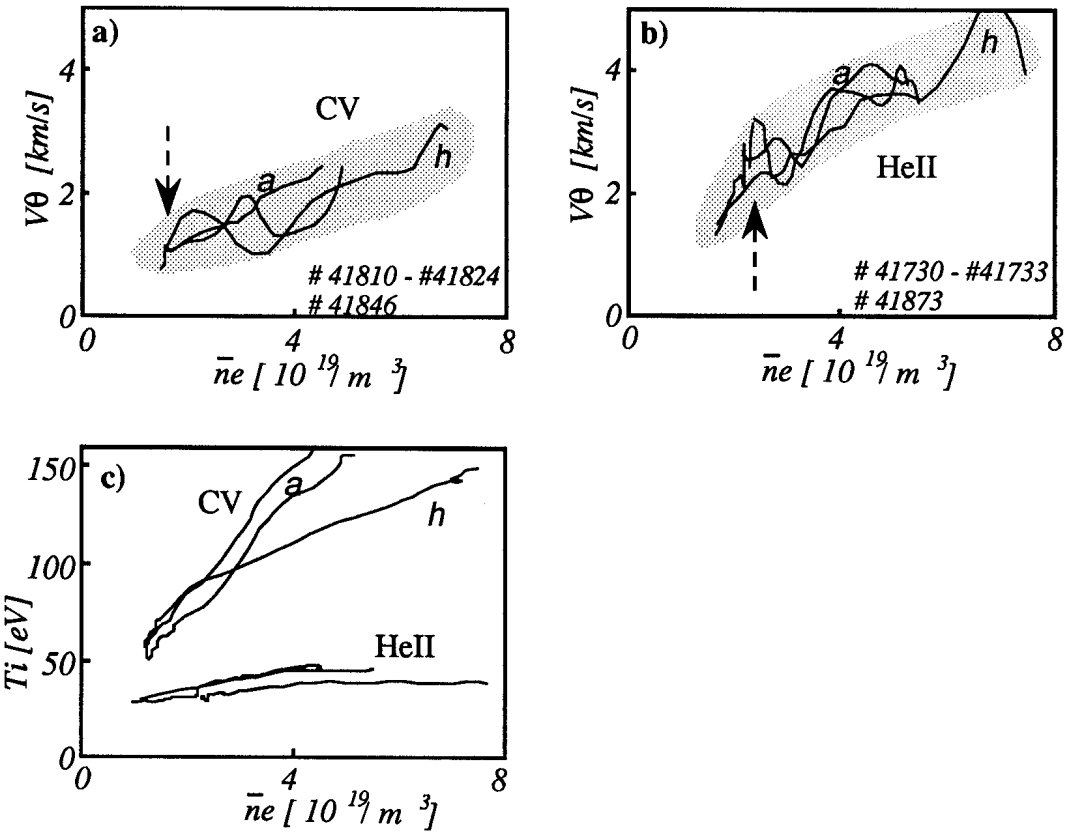

Figure 13: Summary of the poloidal rotation from a) CV and b) HeII shown as a function of the mean plasma density. In each figure, three discharges are shown. The lines marked a correspond to a normal gas ramp or AWH, and the lines marked h correspond to discharges with hard gas puffing. The range of values observed during all the experiments in indicated by the shaded region. c) The ion temperatures for all the discharges in a) and b). The CV ion temperature is clearly lowered by the forced gas puffing.

observed during these experiments. The poloidal rotation measured with AWH is seen to fall in this region. The ion temperature evolution with AWH and normal gas puffing is also very similar, but a strong divergence of the CV ion temperature with hard gas puffing was observed. Thus, even though the plasma ion temperature and the plasma density profiles change significantly, all the results presented fall into the same range.

The variation of poloidal velocity across the minor radius deduced from CV is shown in Figure 14. The poloidal velocity is shown for three similar discharges with the light collected from a chord sampling the outer minor radius (i), the central axis (ii) and the inner minor radius (iii) (see Figure 1). This shows that, to a large degree, the plasma does indeed rotate at a constant velocity in the poloidal direction, at a given minor radius. Data from the edge deduced from CIII and HeII was also self consistent, although the physical access to the line of sight on the inner wall made measurements difficult and the data was not of the same quality. The angular velocity measured at the plasma edge and the CV measurements were similar, but there was some poloidal velocity shear which was observed to vary during and between discharges.

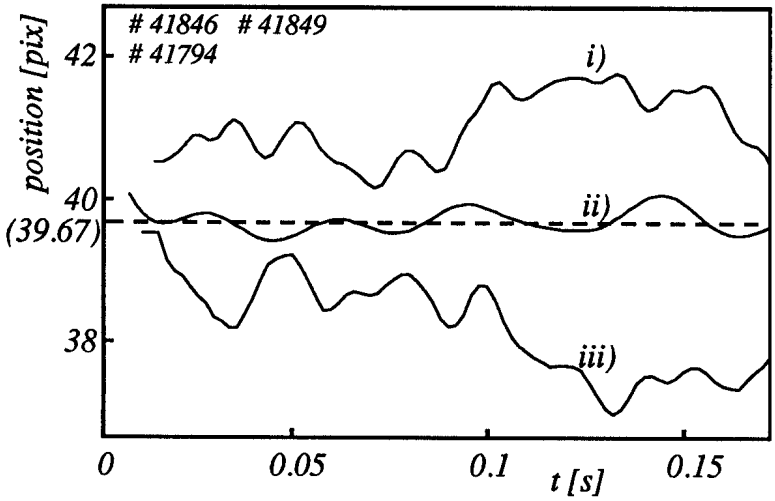

Figure 14: The evolution of the poloidal velocity for similar discharges from CV viewed along three line of sights. i) A tangent to the emission shell on the outer minor radius (chord A figure 1b)). ii) A central line of sight (chord B figure 1b)). iii) A tangent to the emission shell on the inner minor radius (chord C figure 1b)). The plasma is seen to rotate as a rigid body in the poloidal direction. The small lack of symmetry is due to the small differences between the plasma discharges.

One of the main features of AWH is the existence of discrete resonances in the RF spectrum. These resonances, known as DAWs [18], are global and are observed to occur in the density ramp up just before the advent of a new central continuum resonance (see Figure 11). Previous experiments on TCA have shown that even when the plasma density dominated other AWH effects, the DAW, which also causes a peak in the RF power loading, can have a direct effect on the plasma parameters [17] [18]. Although during these experiments, there was often a change in the evolution of the poloidal velocity which occurred close to a DAW, the effect was difficult to parameterise since it could equally be ascribed to the change of the density rather than a direct influence on the rotation velocity. Again, there was no clear evidence of an effect of the RF on the radial electric field.

The characteristic behaviour of changes in the toroidal rotation velocity with strong gas puffing has already been described. The corresponding effect on the poloidal rotation velocity was found to be strongly characterised by the initial phase of the density ramp. In Figure 15, the evolution of several plasma parameters are plotted together with the normalised poloidal rotation velocity for a discharge with hard gas puffing. The parameters evolve smoothly up to the start of the gas puff which is indicated by a vertical line. The locus of the normalised velocity then undergoes a transition which halves its value, indicated by a second vertical line. This transition, which takes place when the density ramp rate is greatest, is accompanied by increased magnetic activity, and a local peak in the value of $d(\beta + li/2) / dt$ which implies that there is a profile change. That the importance of this

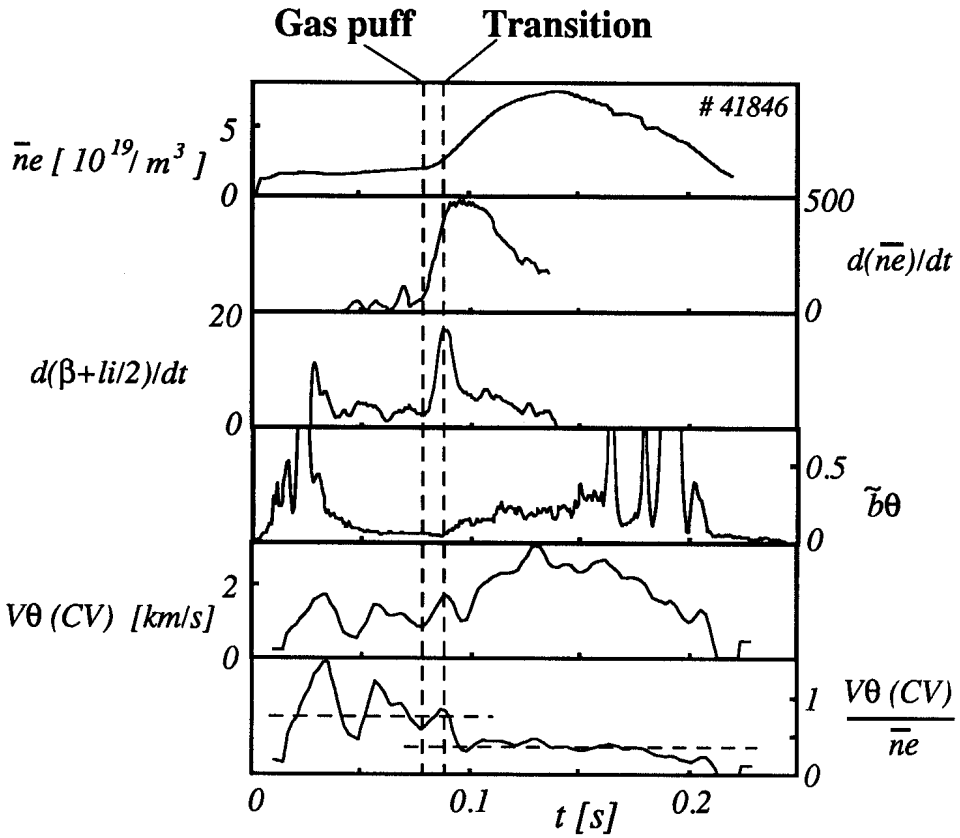

Figure 15: Evolution of several plasma parameters with strong gas puffing. The start of gas puffing is shown by a vertical line. During the period where the density ramp rate is highest, a transition is observed, indicated by a second vertical line, which is co-incident with a peak in $d(\beta+l_i/2)/dt$. The value of the poloidal velocity normalised to the mean plasma density is halved across this transition which is also accompanied by a smooth increase in the magnetic activity.

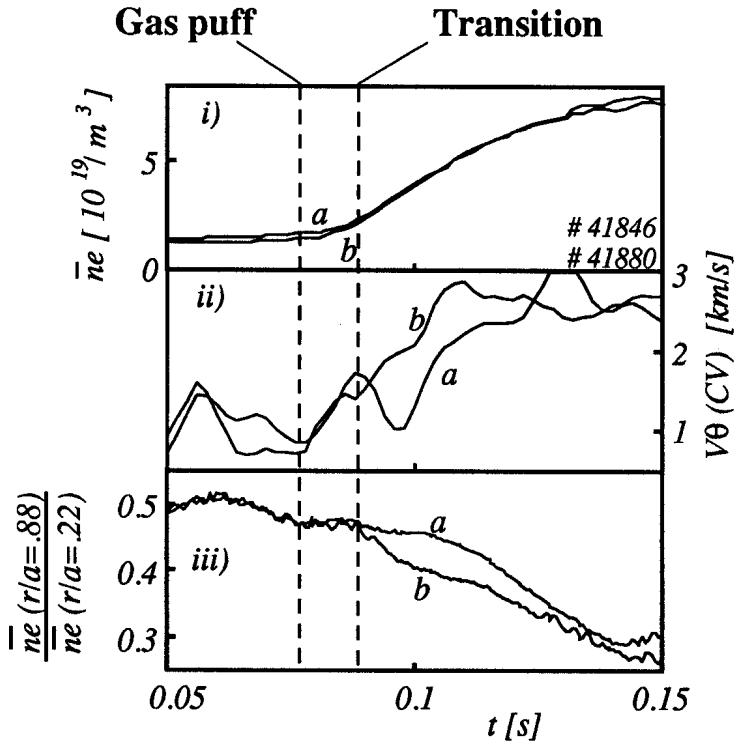

Figure 16: The poloidal rotation evolution is shown for two discharges (ii) with similar plasma density evolutions (i). The discharge with the highest density ramp rate does not undergo the transition shown in Figure 15, which implies this transition also depends on another parameter. iii) The ratio of the line integrated density from an edge chord and a central chord of the FIR interferometer, used to parameterise the peakage of the density profiles for the two discharges. The discharge that shows the transition corresponds to a lower poloidal velocity, and thus radial electric field, and has a less peaked density profile. The two traces rejoin each other at the same time as the poloidal velocities meet.

transition critically depends on the initial density, as well as the density ramp rate, is demonstrated in Figure 16.

Here the results of two discharges with similar density evolutions are shown together with the corresponding poloidal velocities. The discharge which shows a transition is not the one with the largest value of d(ne)/dt. Figure 16 also shows a parameterisation of the density profile peaking factor obtained from the multichannel FIR interferometer. The density in an edge chord (r/a=0.22) is shown normalised to a central chord (r/a=0.88), so that a higher value corresponds to a less peaked density profile. These graphs show that in the transition region, there is a broadening of the density profile which occurs simultaneously with a change in the poloidal velocity and thus the radial electric field. In fact, as the plasma density evolution approaches its apex, the peaking factors for the discharges become similar and the deduced electric fields rejoin each other. Since, with the density ramp, the toroidal velocity is very low, and the effect of the ion density gradient in (1) is considerably lower for CV than at the edge, the increased peaking in the density profile is directly interpreted as an increasing radial electric field.

As a final example of a strong density rise, Figure 17 shows the effect on the toroidal plasma rotation of the injection of a single frozen gas pellet into the flat top of a TCA discharge with Ip=90kA. The pellet causes a jump of a factor of three in the plasma density and the toroidal rotation reacts by immediately stopping. As the plasma density falls, the plasma resumes its toroidal rotation, and recovers its pre-pellet value at approximately the same plasma density. Even across such a violent density change, the toroidal velocity evolution is similar to a gas puff.

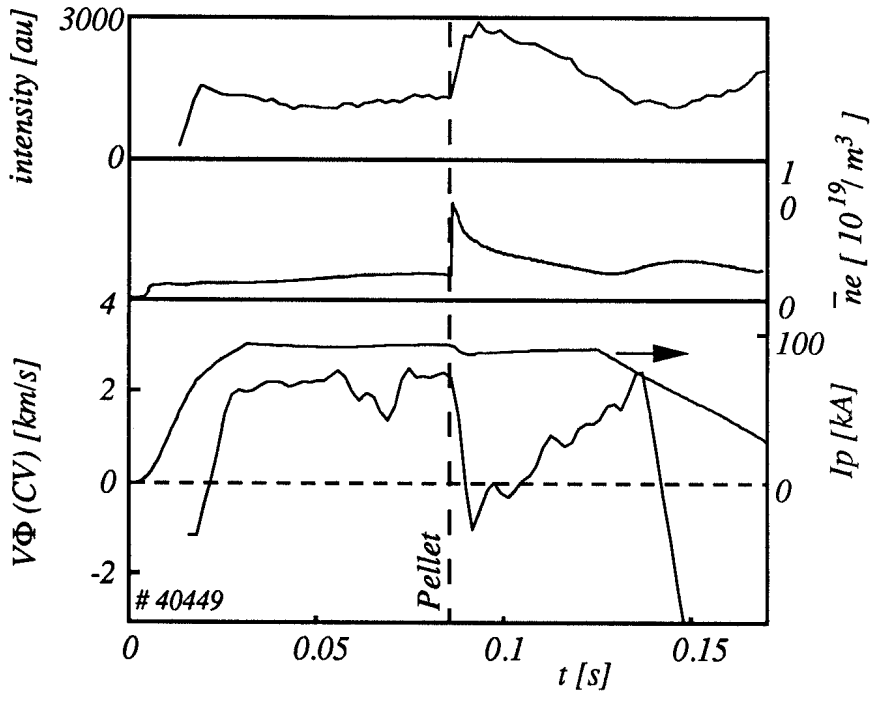

Figure 17: The evolution of the toroidal rotation from CV with pellet injection. The plasma density and plasma current are shown together with the poloidal rotation and line intensity. The pellet increases the plasma density by a factor of 3 and the plasma ceases to rotate toroidally. As the density falls, the plasma accelerates toroidally, recovering its pre-pellet value at the pre-pellet plasma density. During the plasma current ramp down, the plasma accelerates quickly in the opposite direction.

In contrast, the poloidal rotation is not greatly affected by pellet injection. Figure 18 shows the plasma parameters and rotation velocity across pellet injection measured from HeII. Although the plasma density rises significantly, the poloidal velocity remains relatively constant, or even falls slightly, until the plasma current begins to fall. This implies that the radial electric field does not change. Even with the large rate of change of plasma density with forced gas puffing, the radial

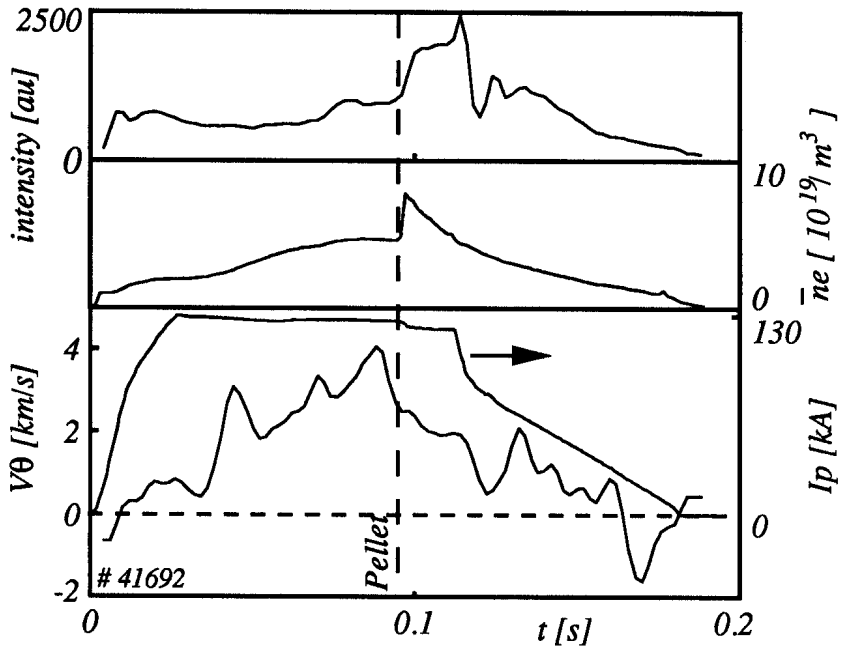

Figure 18: The poloidal rotation measured from HeII with pellet injection. Although the plasma density rises very sharply with pellet injection, the poloidal velocity remains essentially constant. This implies that the radial electric field can not react to the pellet injection, which may explain the fast loss of the plasma density introduced by the pellet.

electric field was observed to follow the density. The radial electric field following injection is thus not what would be expected from the other results. If the radial electric field at a given plasma density is considered to parameterise the particle confinement, albeit with some dependence on the density profile, this could explain the fast density loss following a pellet as the radial electric field prior to the pellet remains frozen in the plasma. It is interesting to note that the plasma density was often observed to fall rapidly to the pre-pellet value where the constant poloidal velocity, and thus radial electric field, was again in agreement with the gas puffing results.

The difference in the behaviour of the toroidal and poloidal velocities is very clear. The plasma appears to be free to stop and accelerate slowly in the toroidal direction whereas in the poloidal direction, such a change implies a more drastic change in the plasma itself.

6. Conclusions

A high quality measurement ($\sigma < 0.12$km/s) of the toroidal and poloidal rotation velocities has been performed on TCA which has been used to deduce the radial electric field. A dominant new source of systematic error in the spectrometer read out method was identified, in which an intensity fluctuation of the observed spectral line results in a systematic error on the measured line centroid. A simple algorithm has been described which was able to reduce the effect of this error on the centroid uncertainty to the level of the residual uncertainty of the whole experimental system. A statistical analysis of the residuals concluded that the experimental uncertainty in the velocity for a spectral line with sufficient intensity was $\sigma \sim 0.12$km/s which is more than an order of magnitude smaller than the velocities observed.

These experiments took place during the final stage of operation before TCA was shut down and, as a result, the range of experimental parameters examined was sometimes restricted by the available operational time. The evolution of the poloidal and toroidal plasma rotation was however measured in a large range of dynamic conditions and it was possible to identify the general behaviour as a function of the strength of the neutral gas feed.

The toroidal velocity was observed to diminish and change sign with increasing plasma density. With hard gas puffing, the rotational direction dynamically reverses before again tending to zero. The plasma edge has a reaction which is both faster and larger than the plasma bulk, an effect which reverses during the plasma current ramp down at the end of the discharge. The toroidal velocity during Alfvén Wave Heating was observed to behave similarly to a normal gas puff, although with higher power AWH, some of the hard gas puffing behaviour became visible. This behaviour was also observed for a very fast density rise caused by pellet injection, and may thus be concluded to be intrinsic to the TCA plasma.

In general, the poloidal rotation was observed to scale with the plasma density. No significant departure from this rule was observed during AWH, and the deduced radial electric field did not show a change which could cause the density rise, which still remains unexplained. As the plasma density rises with AWH, a discrete Alfvén resonance, the DAW, occurs. This resonance did show some signs of modifying the subsequent radial electric field but the effect was not clearly systematic.

During discharges with forced gas puffing, there is a transition in the poloidal rotation normalised to the plasma density which corresponds to a reduced radial electric field. When this transition occurred, there was an accompanying broadening of the plasma density profile which would be expected if the radial electric field is, at least, partially responsible for the inward particle flux. Thus, to some degree, a given plasma density corresponds to a given the poloidal velocity, or radial electric field, albeit with some dependence on the plasma density profile.

The effect of a very sharp increase in the plasma density caused by pellet injection is very informative. Although the toroidal rotation is very quickly damped, there is little effect on the poloidal velocity. The behaviour of the deduced radial electric field was similar with all levels of gas feed, but did not adapt to the very fast density rise accompanying pellet injection. The fast particle loss following pellet injection could be related to radial electric field which remains close to its pre-pellet value.

By observing the plasma along an optimum line of sight and by paying special attention to the experimental technique and error analysis, the plasma rotation velocities have been measured with sufficient precision to allow subtle details of the evolution of the radial electric field to be observed. In a circular machine the size of TCA, with no additional heating, where the rotation velocities are considerably lower than that observed with neutral beam injection, this precision was required to measure the behaviour of the rotation velocities. Both the toroidal and poloidal measurements have shown behaviour which can be divided into general regimes with a smooth transition in between. Although a lot of recent theoretical and experimental work has focussed on the complex phenomena associated with L-H transitions, the observed behaviour in the relatively simple conditions of a circular and ohmically heated plasma already has much information that is unexplained.

Acknowledgments

The authors wish to thank the whole TCA group for its technical support and advice, and in particular Ch. Nieswand for the plasma density profile data. This work was partially supported by Le Fonds National Suisse de la Recherche Scientifique.

References

[1] LISTER J.B. and TCA group, proceeding of IEAEA conference, Kyoto (1987)

[2] CHEETHAM A.D., HEYM A., HOFMANN F., HRUSKA K., KELLER R., LIETTI A., LISTER J.B., POCHELON A., RIPPER H., SIMIK A., TUSZEL A., Proceedings of the 11th Symposium on Fusion Technology 1981

[3] NOWAK S.,JOYE B., MARMILLOD PH., Rev. Sci. Instrum 57 (1986), 19

[4] IDA K.,HIDEKUMA S., MIURA Y., FUJITA T., MORI M., HOSHINO K., SUZUKI N., YAMAUCHI T., and JFT-2M Group, Phys. Rev. Lett. 65, (1990), 11

[5] GROEBNER R.J., BURRELL K.H., SERAYDARIAN R.P., Phys. Rev. Lett. 64, (1990), 2369

[6] TAYLOR R.J., BROWN M.L., FRIED B.D., GROTE H., LIBERATI J.R., MORALES G.J., PRIBYL P., DARROW D., ONO M., Phys. Rev. Lett. 63, (1989), 21

[7] STRINGER T., Phys. Rev. Lett. 22, (1969), 770

[8] DUVAL B.P., JOYE B., MARCHAL B., to be submitted (1991)

[9] PIETRZYK Z.A., POCHELON A., BEHN R., BONDERSON A., DUPERREX P.-A., DUVAL B.P., KNIGHT A.J., MARCHAL B., NIESWAND C., Density Limit Disruption Studies in the TCA Tokamak., Submitted Nucl. Fusion (1991).

[10] EG&G Reticon 1024 series S array in OMA III detector

[11] HAWKES N., BREGER P., CAROLAN P., GIANELLA R., MORGAN P., PEACOCK N., STAMP M., JET internal report JET-IR(91)03 April 1991

[11] GROEBNER R.J., BURRELL K.H., GOHIL P.,SERAYDARIAN R.P., Proc. 8th Top. Conf. High Temp. Plas. Diag. Hyannis (1990) and GA report GA-A20200, October 1990

[12] HOLLENSTEIN Ch., DUVAL B.P., DUDOK de WIT T., JOYE B., KUNZLI H.J., OELHAFEN P., ZEHRINGER R., HAUERT R., MOSER E.M., Journ. Nucl. Mater. 176 & 177 (1990) 343-349

[13] BENJAMIN R.D., TERRY J.L., MOOS H.W., Phys. Rev. Lett. 41, (1990), 1034-1040

[14] HAWKES N., BREGER P., CAROLAN P., GIANNELLA R., MORGAN P., PEACOCK N., STAMP M., Jet Report JET-IR(91)03, April 1991

[15] FIELD A.R., FUSSMANN G., HOFFMANN J.V. Report IPP III/165 (1990), partially published Proc.18th EPS Berlin (1991) 1556 -1559

[16] WEISEN H., BORG G., JOYE B., KNIGHT A.K., LISTER J.B., Phys. Rev. Lett. 62, (1989), 4

[17] DE CHAMBRIER A., DUVAL B.P., LISTER J.B., MOMPEAN F.J., MORET J.-M., Plas. Phys. and Cont. Fusion 31, (1989), 4

[18] COLLINS G.A., HOFMANN F., JOYE B., KELLER R., LEITTI A., LISTER J.B., POCHELON A., Phys. Fluids 29, (1986), 7